UNDERWATER IMAGE DE-SCATTERING AND ENHANCING USING DEHAZENET AND HWD

Pan-wang Pan
Key Laboratory of Underwater Acoustic Communication and Marine Information Technology Ministry of Education, Xiamen University, Xiamen, Fujian, China.

Fei Yuan
Key Laboratory of Underwater Acoustic Communication and Marine Information Technology Ministry of Education, Xiamen University, Xiamen, Fujian, China., yuanfei@xmu.edu.cn

En Cheng
Key Laboratory of Underwater Acoustic Communication and Marine Information Technology Ministry of Education, Xiamen University, Xiamen, Fujian, China.

UNDERWATER IMAGE DE-SCATTERING AND ENHANCING USING DEHAZENET AND HWD

Acknowledgements

UNDERWATER IMAGE DE-SCATTERING AND ENHANCING USING DEHAZENET AND HWD

Pan-wang Pan, Fei Yuan, and En Cheng

Key words: convolutional neural network, adaptive bilateral filter, hybrid wavelets and directional filter banks.

ABSTRACT

De-scattering and edge enhancing are critical procedures for underwater images which suffer from serious contrast attenuation, color deviation, and edge blurring. In this paper, a novel method is proposed to enhance underwater images. Firstly, a Convolutional Neural Network (CNN) is trained end-to-end to estimate the transmission map. Simultaneously, the adaptive bilateral filter is used to refine the transmission map. Secondly, a strategy based on the white balance is proposed to remove the color deviation. Laplace pyramid fusion is utilized to obtain the fusion result of the haze-free and color-corrected image. Finally, the output image is transformed into the Hybrid Wavelets and Directional Filter Banks (HWD) domain for de-noising and edge enhancing. The experimental results show that the proposed method can remove color distortion and improve the clarity of the underwater images. Objective and subjective results demonstrate that the proposed method outperforms several state-of-the-art methods in different circumstances.

I. INTRODUCTION

Underwater imaging has played a crucial role in marine resource exploration, environmental protection, maritime defense and military affairs, etc. However, underwater images suffer from the poor visibility resulting from back-scattering and light attenuation. Random attenuation of light causes the foggy appearance. A part of light scattering back from the medium along the sight degrades the contrast of captured images. In different underwater environments, the main reason for image degradation is different.

Recently, researchers have proposed several methods to improve the quality of underwater images. Polarization and range-gated imaging methods (Schechner and Karpel, 2005; Tan et al.,

2007) addressed this issue by specialized hardware directly. Another method studied in (Voss et al., 1990) measured the optical transfer function of seawater. The Modulation Transfer Function (MTF) of seawater was formulated in (Liu et al., 2001), and blurred images can be restored by the Wiener filter. However, above mentioned experimental methods were inapplicable to most of ocean engineering applications and scientific researches due to expensive cost and complicated configuration of the equipment. De-convolution methods based on underwater degeneration models are flawed in practical applications due to complex and changeable underwater environments.

In addition, image enhancement methods do not rely on any specific degeneration model, and they deal with images according to the human visual perception. Common enhancement methods consist of traditional histogram correction (Thakur et al., 2010), gradient transformation (Lei et al., 2011) and some other adaptive smoothing methods, such as traditional low-pass filter, morphological filter, homomorphic filter (Padmavathi et al., 2011), wavelet transform, etc. Iqbal et al. (2010) proposed an unsupervised color correction method to improve the visual quality of underwater images. Ancuti et al. (2012) proposed a fusion-based method to enhance underwater videos and images. However, image enhancement methods might cause color deviation and show their limitations when dealing with underwater images.

The haze removal algorithm is used for underwater image restoration method. He et al. (2009) estimated the transmission map of degraded images by Dark Channel Prior (DCP) and obtained clear images by atmospheric imaging model. Furthermore, the guided filter (He et al., 2010) was developed to refine the raw transmission map. Drews-Jr. et al. (2013) formulated an underwater imaging model that calculates the dark channel by blue and green channels. To avoid extracting features artificially, Cai et al. (2016) estimated the transmission map via a deep learning architecture.

In this paper, we propose an approach which is able to increase the visibility of underwater images. It improves the contrast of scattered images by DehazeNet and white balance and then enhances edges in image. Fig. 1 depicts the schematic diagram of our algorithm. Firstly, we apply a type of CNN named DehazeNet to estimate the underwater transmission map which is refined by an adaptive bilateral filter. Secondly, we develop a framework to blend the de-hazed and color-corrected image.
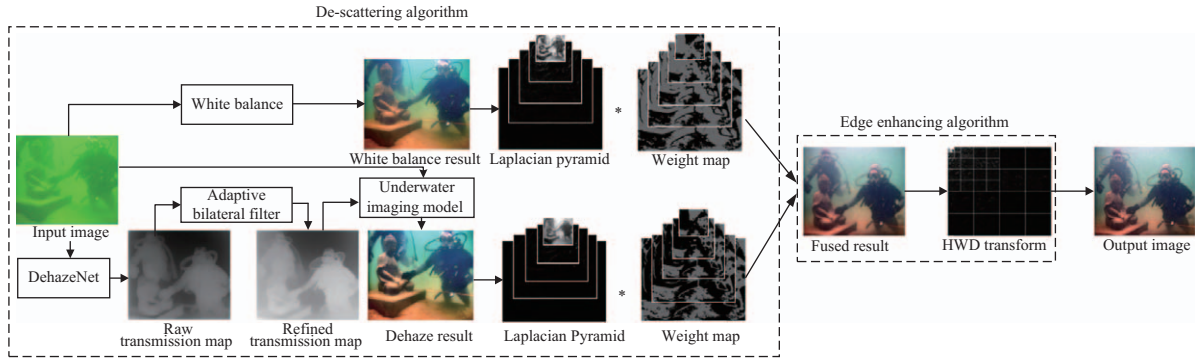
Fig. 1. The schematic diagram of our approach.

Finally, we separate the high-frequency and low-frequency components of image by the hybrid wavelets and directional filter banks. In the HWD domain, the noise variance is estimated by the high-frequency subbands and the threshold is set to remove the noise. Furthermore, an edge enhancement algorithm is applied to the de-noised image.

The rest of this paper is organized as follows: a de-scattering algorithm is formulated in Section 2, and an edge enhancement algorithm is provided in Section 3. A non-reference image quality assessment for the analysis of original and enhanced images is formulated in Section 4. Corresponding experiment results are presented in Section 5, and conclusions are drawn in Section 6.

II. DE-SCATTERING ALGORITHM

1. Underwater Imaging Model

Inspired by the atmospheric scattering model, the underwater imaging model (Chao et al., 2010) can be expressed as

$$I(x) = J(x)t(x) + B(x)(1 - t(x)) \qquad (1)$$

where $I(x)$ is an observed image, $J(x)$ is a clear image, $B(x)$ is the background light, and $t(x)$ is the transmission map.

In underwater environments, light suffering from absorption and scattering will disappear one by one depending on the depth of water. Approximately, red light disappears at a depth of 3 m and yellow light disappears at a depth of 10 m. With the increasing of depth, only blue and green light will exist due to their shorter wavelength. Therefore, underwater images are dominated by blue and green color. The underwater dark channel of $J(x)$ is calculated by blue and green channels according to the Underwater Dark Channel Prior (UDCP).

$$J_{dark}(x) = \min_{C \in (g,b)} \left(\min_{y \in \Omega(x)} J^C(y) \right) \qquad (2)$$

where $\Omega(x)$ is a patch centered at x. $J^C(y)$ is color channel C of $J(y)$.

We pick top 0.1% brightest pixels in the underwater dark channel. Corresponding pixels in the observed image are selected as the background light of green and blue channels.

$$B^C(x) = I^C(\arg\max J_{dark}(x)), \, x \in P_{0.1\%}, \, C \in \{g, b\} \qquad (3)$$

In the red channel of observed image, pixels of the top 0.1% highest intensity are used as the background light of red channel and can be expressed as

$$B^C(x) = I^C(x), \, x \in P_{0.1\%}, \, C \in \{r\} \qquad (4)$$

The final clear image is recovered by

$$J(x) = \frac{I^C(x) - B^C(x)}{\max(t_0, t(x))} + B^C(x), \, C \in \{r, g, b\} \qquad (5)$$

where a typical value of t_0 is 0.1.

If the input image is distorted seriously, the actual transmission map can't be calculated accurately by traditional models. So we apply a network architecture to estimate the transmission map.

2. Layer Designs of DehazeNet

Convolution layers and nonlinear activations of DehazeNet are designed to implement four sequential operations. It consists of feature extraction, multi-scale mapping, local extremum, and nonlinear regression.

Feature extraction is different from the traditional convolution neural network. In the first layer, DehazeNet uses convolution layer with Maxout activation function (Goodfellow et al., 2013) instead of the Rectified Linear Unit (ReLU), and the specific expression can be generally written as

$$F_1^i(x) = \max_{j \in [1,k]} g^{i,j}(x), \, g^{i,j} = w^{i,j} * I + b^{i,j} \qquad (6)$$

where $w^{i,j}$ and $b^{i,j}$ are the weight and bias of network, respectively; I is the input of DehazeNet; $*$ denotes the convolution operation. The visualization result of convolution kernels shows that the trained convolution kernels can extract features of the opposite filter, all-pass filter and round filter, as shown in Fig. 2.

Since the efficiency of haze removal algorithm will be im-

(a) Opposite filter (b) All-pass filter (c) Round filter (d) The trained convolution kernels
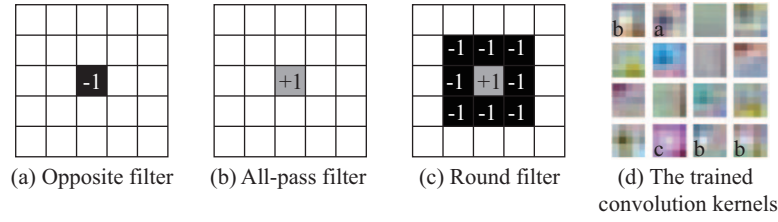
Fig. 2. Filter weight in the first layer.
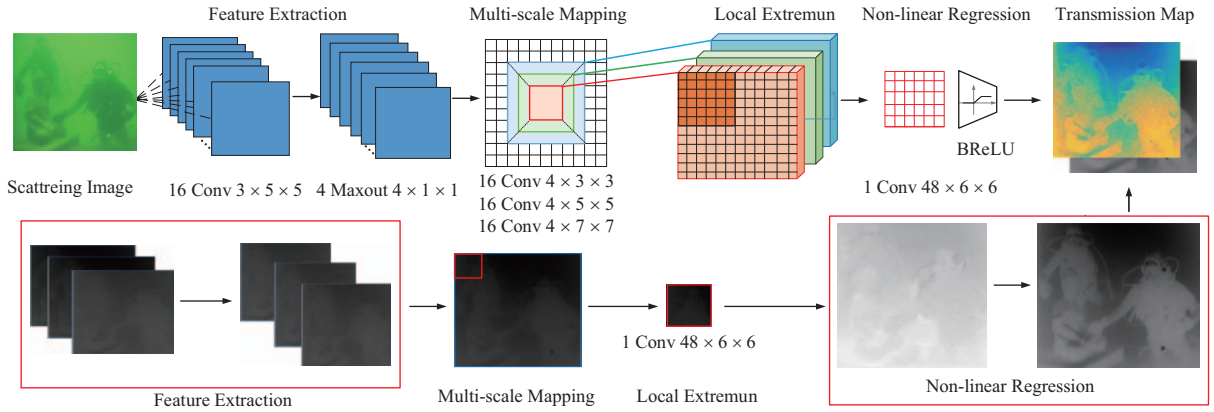
Fig. 3. The schematic diagram of DehazeNet.

proved by multi-scale features (Tang et al., 2014), DehazeNet extracts features with three convolution kernels of different sizes (i.e., 3×3, 5×5, and 7×7). The local extremum constrains the local consistency of the transmittance map and suppresses the noise of the estimated transmittance map. The range of transmission map is from 0 to 1, so this paper makes use of Bilateral Rectified Linear Unit (BReLU) to normalize the network output, as shown in Fig. 3.

In practice, there is no simple way to obtain image pairs of corresponding clear and hazed images for training. So we create a synthetic dataset of 5,319 clear/hazed image pairs , as shown in Fig. 4. The hazed images are generated according to underwater imaging model described in Eq. (1).

3. Adaptive Bilateral Filter

The adaptive bilateral filter is utilized to refine the blocking artifacts of the transmission map. The bilateral filter (Morillas et al., 2006) is based on a non-iterative method which has been proven to preserve the texture structure of image effectively. The expression of bilateral filter can be expressed as

$$I_{BF}(p) = \frac{1}{W_p} \sum_{q \in \Omega(p)} G_s(\| p - q \|) G_r(\| I(p) - I(q) \|) I(q) \quad (7)$$

where $\Omega(p)$ is an image patch centered at p, W_p is the normalization factor. It can be formulated as follows

$$W_p = \sum_{q \in \Omega(p)} G_s(\| p - q \|) G_r(\| I(p) - I(q) \|) \quad (8)$$

where G_s and G_r are Gaussian function. Their formulas are shown as follows, respectively.

$$G_s(\| p - q \|) = \exp(-\frac{\| p - q \|^2}{2\sigma_s^2}) \quad (9)$$

$$G_r(\| I(p) - I(q) \|) = \exp(-\frac{\| I(p) - I(q) \|^2}{2\sigma_r^2}) \quad (10)$$

where G_s is a smoothing kernel to measure the spatial similarity of pixels. It is shown that the weight of the bilateral filter is proportional to the spatial similarity. Pixels in the smooth region have a stronger correlation than pixels in the edge region. Therefore, pixels in the edge region can be kept well while removing noise.

The adaptive bilateral filtering is proposed to choose the σ_r automatically. It selects the σ_r by calculating the variance of image patches σ_{blk}. Simultaneously, we set the upper and lower bounds. The formula is described as

$$\sigma_r = \max(\sigma_{r,\min}, \min(\sigma_{r,\max}, k\sigma_{blk})) \quad (11)$$

where $\sigma_{r,\max}$ and $\sigma_{r,\min}$ are the upper and lower bound respectively, and K is a positive number. In this paper, we set $\sigma_s = 6$, $\sigma_{r,\min} = 1$, $\sigma_{r,\max} = 10$, $k = 6$.

4. White Balance

White balance is an algorithm for removing unrealistic color

(a)	(b)	(c)	(d)
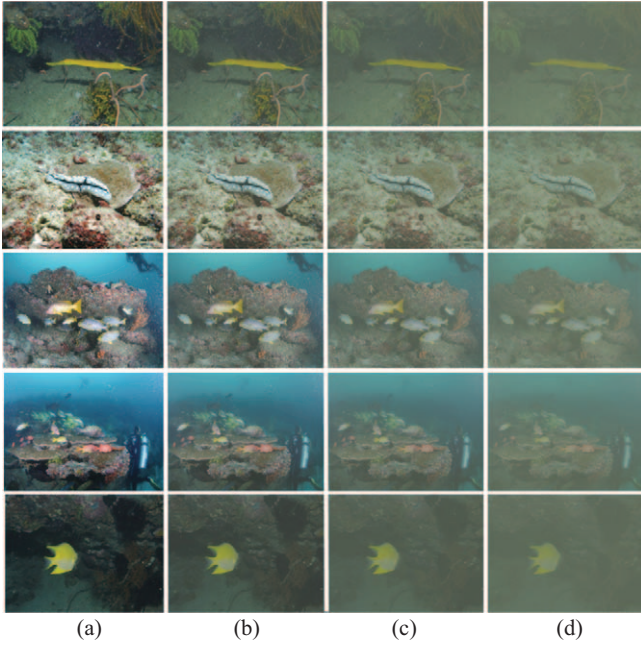
Fig. 4. (a) Clear images and (b)-(d) simulated underwater images.

deviation and can be roughly classified into two steps: light estimation and color correction.

In the first step, the Shades-of-Grey (Finlayson et al., 2004) method is applied. This method calculates the illumination of the scene for each color channel by the Minkowski p-norm. When $p = 1$, this expression is a particular case of the Gray-World. It is not suitable for underwater images because the red component of underwater images is missing. When $p = \infty$, it has the same effect with White-Patch hypothesis. It does not work in underwater environments because it relays on white objects in underwater images. In our experiments, the Shades-of-Grey algorithm can estimate the light effectively when $p = 6$.

In the step of color correction, we apply Robust-AWB (Huo et al., 2006) to correct color deviation of severe underwater images after a comprehensive comparison. This algorithm searches for gray pixels in the image and compares the deviation of these gray pixels in the YUV color space. Through the iterative procedure, it corrects color deviation gradually.

2. Laplacian Pyramid Fusion

We define $I(x, y)_1$ and $I(x, y)_2$ to represent the de-hazed and color-corrected result of the original underwater image, respectively. Each input is decomposed into different scales by the Laplacian pyramid. Each normalized weight map is formulated in (Ancuti et al., 2012). The enhanced image is obtained by

$$R^l(x, y) = \sum_{k=1}^{2} G^l\{W(x, y)_k\} L^l\{I(x, y)_k\} \quad (12)$$

where l is the number of the pyramid levels (the typical value is 5), $L\{I\}$ represents the Laplacian version of the input I, and

$G\{W\}$ represents the Gaussian version of the normalized weight map W. By inputting images of different resolution, results of using Laplacian pyramids will be more robust than results without Laplacian pyramids.

III. EDGE ENHANCEMENT ALGORITHM

1. HWD Transform

The traditional two-dimensional Discrete Wavelet Transform (DWT) only captures information in limited directions (i.e., horizontal, vertical, and diagonal directions). Therefore, DWT is generally inadequate for representing geometric structures of underwater images. Eslami et al. (2007) proposed a new family of no redundant geometrical image transform based on hybrid wavelets and directional filter banks. It applies Directional Filter Banks (DFB) to the high-frequency wavelet subbands and maintains the information of image contour and textures. Therefore, HWD transform can provide a richer family of directional basis elements than discrete wavelet transform.

In the HWD transform, underwater images are decomposed into L levels by the DWT, and directional filter banks are applied to high-frequency subbands. Since the HH wavelet subbands maintain major high-frequency information, Full-tree DFB (FDFB) is applied to HH wavelet subbands. The horizontal information of high-frequency is mainly distributed in the HL wavelet subbands, so the Horizontal half-tree DFB (HDFB) is applied to the HL wavelet subbands. Similarly, the Vertical half-tree DFB (VDFB) is applied to the LH wavelet subbands.

The direction angle of the i-th direction subband is defined as the angle between the filtering direction and the horizontal axis. Angles of FDFB, HDFB and VDFB are expressed as

$$\theta_F(i) = \begin{cases} (1/4 + 1/2^{L+1} - i/2^L)\pi, & 1 \le i \le 2^{L-1} \\ -(1/4 + 1/2^{L+1} - i/2^L)\pi, & 2^{L-1} + 1 \le i \le 2^L \end{cases} \quad (13)$$

$$\theta_H(i) = -(1/4 + 1/2^{L+1} - i/2^L)\pi, 1 \le i \le 2^{L-1} \quad (14)$$

$$\theta_V(i) = (1/4 + 1/2^{L+1} - i/2^L)\pi, 1 \le i \le 2^{L-1} \quad (15)$$

where L is the layer number of wavelet transform. After the discrete wavelet transform, the frequency distribution and the three direction filter banks are shown in Fig 5.

We transform underwater images into wavelet domain by the Cohen-Daubechies-Feauveau (CDF) 9/7 wavelet transform and compare with the coefficients of the HWD transform, as shown in Fig. 6. By observing the coefficients of the CDF 9/7 and HWD transform, the coefficients of HWD transform are larger than the coefficients of CDF 9/7 transform, especially in high-frequency subbands. Thus, we draw the conclusion that HWD transform captures more information of texture and contour details.

2. Denoise and Edge Enhancement

The high-frequency coefficients of the first layer are used to
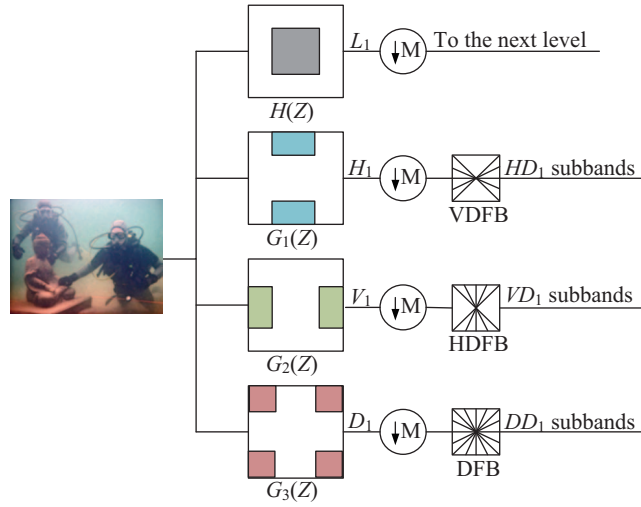
Fig. 5. The schematic diagram of HWD transform.

(a) (b) (c)
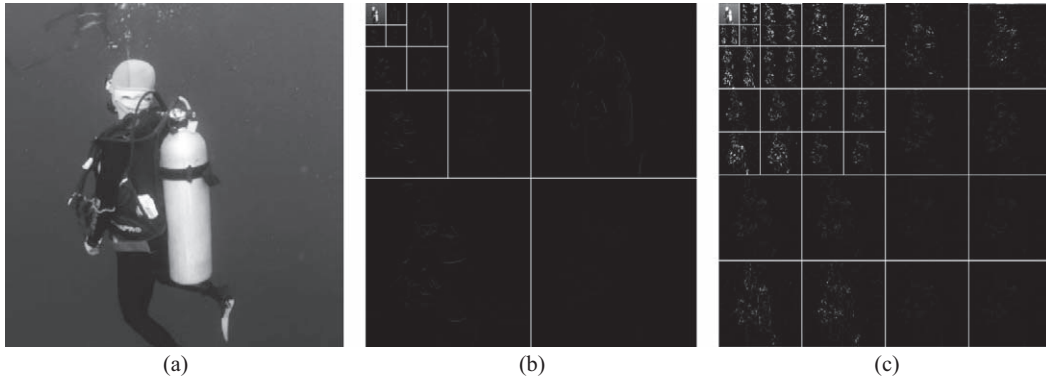
Fig. 6. (a) Underwater image with (b) four-level 9/7 wavelet transform and (c) four-level HWD-F transform.

estimate the noise variance of the input image. And then we apply the denoising pretreatment based on the wavelet threshold method, and the threshold T_k can be derived as follows

$$T_k = \frac{1}{2}\sqrt{\frac{1}{m \times n}\sum_{x=1}^{m}\sum_{y=1}^{n}[P_k(x, y) - \overline{P}]^2} \qquad (16)$$

where $\overline{P}$ is the mean of the wavelet coefficients in first layer. The coefficients smaller than the threshold are regarded as noise. While the coefficients larger than the threshold are regarded as blurred edges. Then the coefficients of HWD transform HH_i, LH_i, HL_i are multiplied by coefficients K_i ($K_i > 1$) for enhancing blurred edges. As the number of decomposition layers i increases, the corresponding coefficients K_i decrease gradually.

IV. NON REFERENCE IMAGE QUALITY ASSESSMENT

1. Gray-Level Co-Occurrence Matrix

In this paper, we use a Non-Reference (NR) quality evalua-

(a) (b)
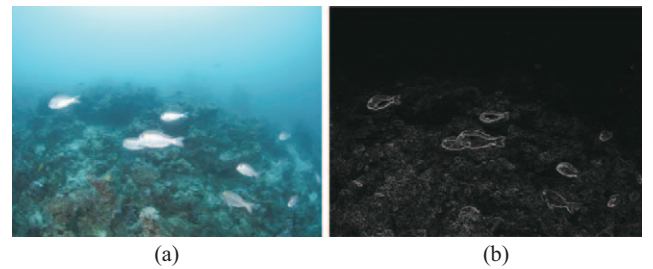
Fig. 7. (a) Original image. (b) Gradient image.

tion algorithm based on gray-level co-occurrence matrix (Sang et al., 2013) to evaluate the results of different algorithms. The gradient image of the original image reflects the loss of texture and contour details as shown in Fig. 7.

On the basis of the gradient image, the gray-level co-occurrence matrix (GLCM) is introduced, and the texture features of distorted and restored images are extracted according to the gray-level co-occurrence matrix. GLCM calculates the contrast, dissimilarity, entropy, homogeneity, and energy to represent the texture features of underwater images.

The formulas of contrast and dissimilarity are given by

$$T_1(f, L, d, \theta) = \sum_{i=0}^{L-1}\sum_{j=0}^{L-1}(i-j)^2\, p\left(i, \frac{j}{d}, \theta\right) \qquad (17)$$

$$T_2(f, L, d, \theta) = \sum_{i=0}^{L-1}\sum_{j=0}^{L-1}|i-j|\, p\left(i, \frac{j}{d}, \theta\right) \qquad (18)$$

Contrast and dissimilarity represent the sharpness of the image. Usually, they are proportional to the sharpness of underwater images.

The formula of entropy can be expressed as

$$T_3(f, L, d, \theta) = -\sum_{i=0}^{L-1}\sum_{j=0}^{L-1}p\left(i, \frac{j}{d}, \theta\right)\log\left(p\left(i, \frac{j}{d}, \theta\right)\right) \qquad (19)$$

The entropy of gradient image reflects how much texture components in the image. Therefore, entropy is proportional to the clarity of underwater images.

The formula of homogeneity is given by

$$T_4(f, L, d, \theta) = -\sum_{i=0}^{L-1}\sum_{j=0}^{L-1}\frac{p\left(i, \frac{j}{d}, \theta\right)}{(1+|i-j|)} \qquad (20)$$

The homogeneity denotes the distribution of elements in the gray level co-occurrence matrix. Therefore, homogeneity is inversely proportional to the clarity of underwater images.

The formula of energy is given by

$$T_5(f, L, d, \theta) = \sum_{i=0}^{L-1}\sum_{j=0}^{L-1}p^2\left(i, \frac{j}{d}, \theta\right) \qquad (21)$$

When the value of the GLCM changes greatly, it indicates that the image is blurred. Thus, energy is inversely proportional to the image quality.

2. Random Forests Regression

We train a random forest by the gray-level co-occurrence matrix {T1, T2, T3, T4, T5} and predicts the Differential Mean Opinion Scores (DMOS) of underwater images by Algorithm 1.

Algorithm 1: The random forests regression algorithm
Initialization:
(a) Gradient images of original images in LIVE2 database are extracted by the gradient transformation.
(b) The feature vector is constructed by GLCM.
Iteration:
(c) We draw n tree bootstrap samples from the original data.
(d) For each of the bootstrap samples, we grow an unpruned regression tree with the following modification: at each node, we

choose the best split among all predictors. Then we sample m of the predictors randomly and choose the best split among those variables.
(e) Random forests predict new data by aggregating the predictions of the n trees.
(f) On the basis of the training data, the error rate of n trees can be obtained.
(g) We obtain the image quality assessment model which substitutes optimization parameters and test the model by Pearson Correlation Coefficient (PCC) and Spearman Rank-Order Correlation Coefficient (SPOCC).

V. EXPERIMENTS

To demonstrate the contributions of this work, we present results from three types of experiments using a series of underwater images. The simulation tool is MATLAB R2015b on a PC with a 3.20GHz Intel Core i5-6500 Processor.

1. Verification of De-scattering Algorithm

To evaluate the effectiveness of the de-scattering algorithm, we test two up-to-date single image haze removal algorithms in scattering images without color distortion, as shown in Fig. 8.

It is obvious that enhanced results which are shown in Fig. 8(d) have the highest subjective quality than other haze removal algorithms, meanwhile, the global appearance of corresponding results are preserved better. This is because the proposed approach is based on the DehazeNet, fusion technology and edge-preserving filter. It not only enhances the texture and contour details, but also can adjust the illumination to make subjective visual perception more comfortable. In addition, traditional haze removal algorithms can't be implemented effectively in some extreme conditions because the transmission map of distorted images cannot be estimated accurately.

Since the white balance technology is included in our algorithm, our approach is capable of working in the scattering images with color distortion. We also compare with the current visibility improving methods based on DCP (Chiang et al., 2012), multi-scale Retinex with color restore (Zhang et al., 2012) and automatic red-channel (Galdran et al., 2015) to further verify the performance of the proposed approach. As the results shown in Fig. 9, Chiang's method begins to lose effectiveness with the addition of color distortion. Zhang's method can improve the contrast to a certain extent, but it brings color deviation. Besides, our approach provides better performance than Galdran's approach in term of the quality of distant objects and background light. More importantly, we have noticed that automatic red-channel algorithm has poor performance in such cases where the appearance is overall blue or green. Restored images of Galdran's approach will show reddish appearance. This is mainly due to the fact that underwater images have lower contrast and less visible edges than natural images. Through the fusion stage, the proposed approach has most stable performance in this case.

We evaluate original images and enhanced results by the above mentioned non-reference quality evaluation model to com-
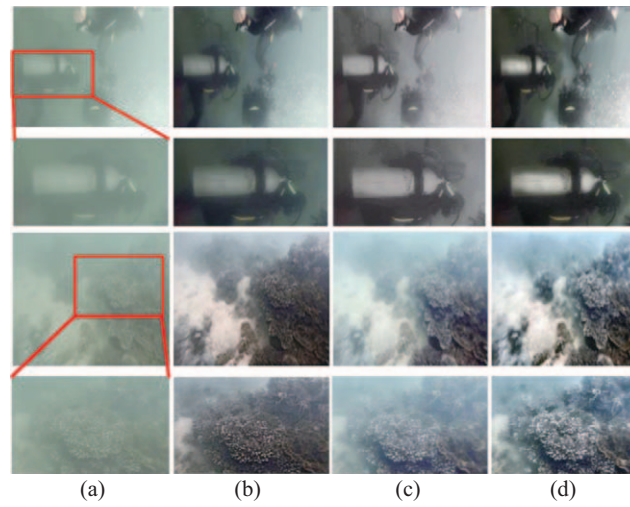
Fig. 8. (a) Original image and Enhanced image by (b) He's approach, (c) Ancuti's approach and (d) the proposed approach.
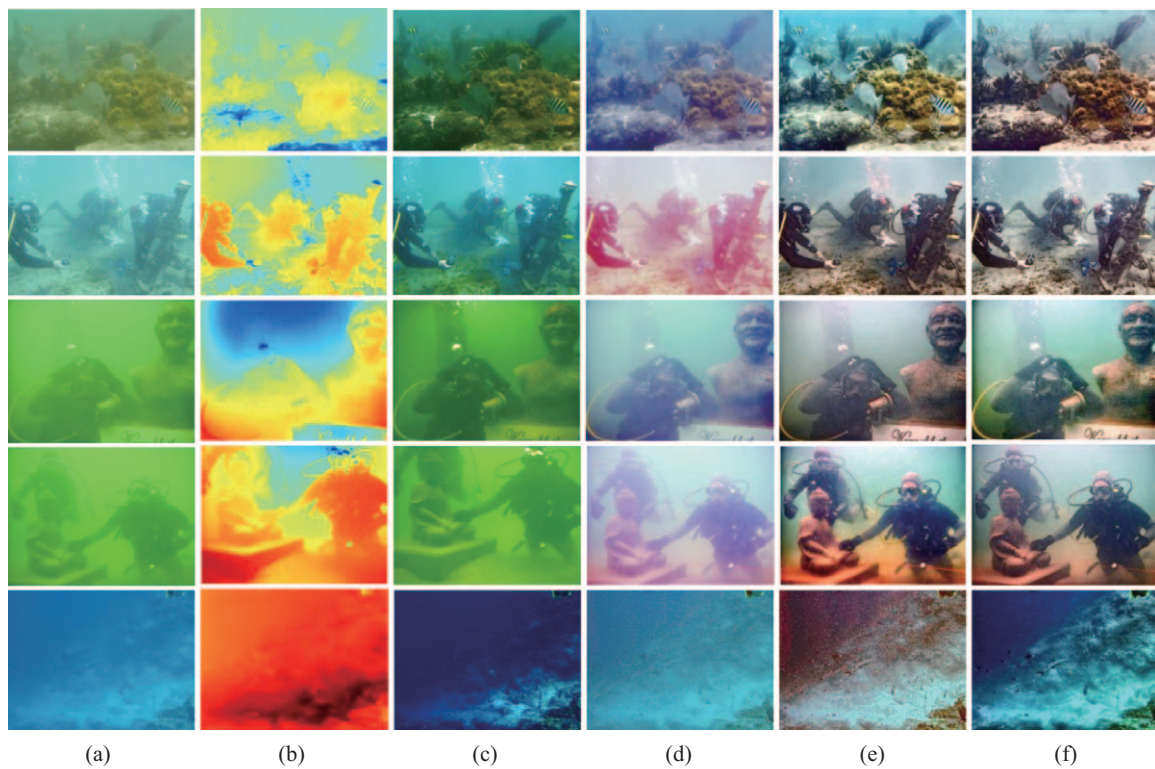
Fig. 9. (a) Original image (b) Estimated transmission map by proposed approach (c) Enhanced image by Chiang's approach(d) Enhanced image by Zhang's approach(e) Enhanced image by Galdran's approach (f) Enhanced image by the proposed approach.

pare with different algorithms quantitatively. The bar charts, where the x-axis is the serial number of the test images, y-axis is the score of each evaluation index, are shown in Fig. 10.

Table 1 lists the predicted DMOS of five test images and enhanced results by the random forests regression. The value of DMOS is inversely proportional to the image quality.

We draw the conclusion from Fig. 10 and Table 1 that evaluation results of five evaluation indexes have the same trend and show that the proposed approach is more effective than other

approaches in term of objective quality score.

2. Verification of Edge Enhancement Algorithm

The proposed approach can enhance other kinds of degraded image, such as optical turbulence blur images. In this experiment, a blind de-blurring method (Pan et al., 2016) is referenced to make a comparison. Fig. 11 shows the experimental results of three blur underwater images.

Since suspended particles in the medium cause light absorp-

Table 1. NR image quality assessment results.

number	Original image	Chiang's approach	Zhang's approach	Galdran's approach	Proposed approach
#1	5.5492	5.3606	5.3508	**1.7501**	1.9214
#2	4.4169	3.3649	4.2649	2.6840	**0.2587**
#3	6.2892	6.0668	4.2143	2.3585	**2.2508**
#4	8.4783	8.2958	8.0667	6.9532	**4.9532**
#5	10.1150	9.9899	9.8582	8.5451	**6.5451**
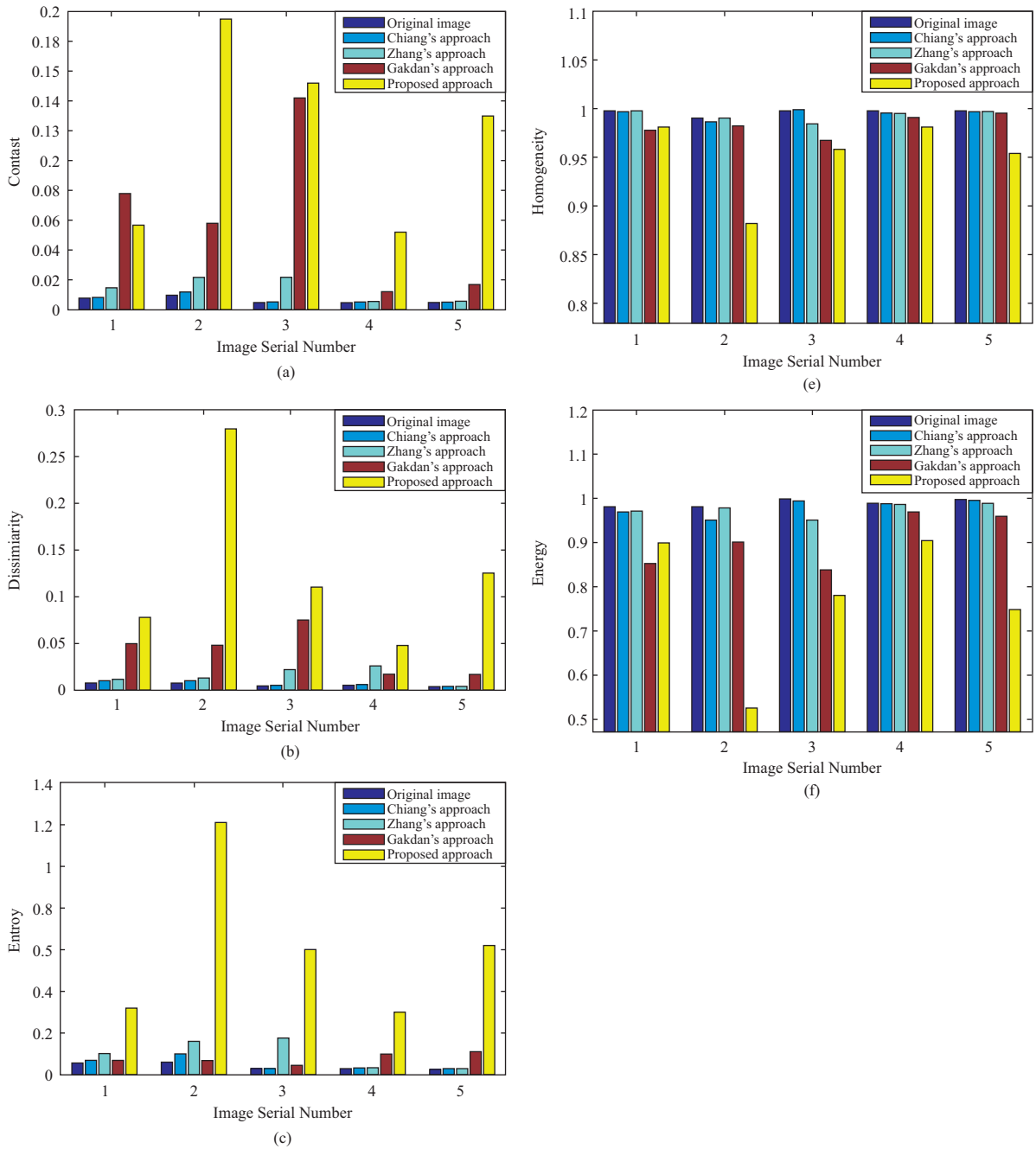
Fig. 10. The (a) contrast, (b) dissimilarity, (c) entropy, (d) homogeneity and (e) energy scores of five test images.

tion, we enhance edges in image to improve its visibility. Fig. 11 shows that contour details of turbulence blur images are enhanced by the proposed method. And the proposed method obtains clearer edges than Pan's method.

| | | |
| (a) | (b) | (c) |
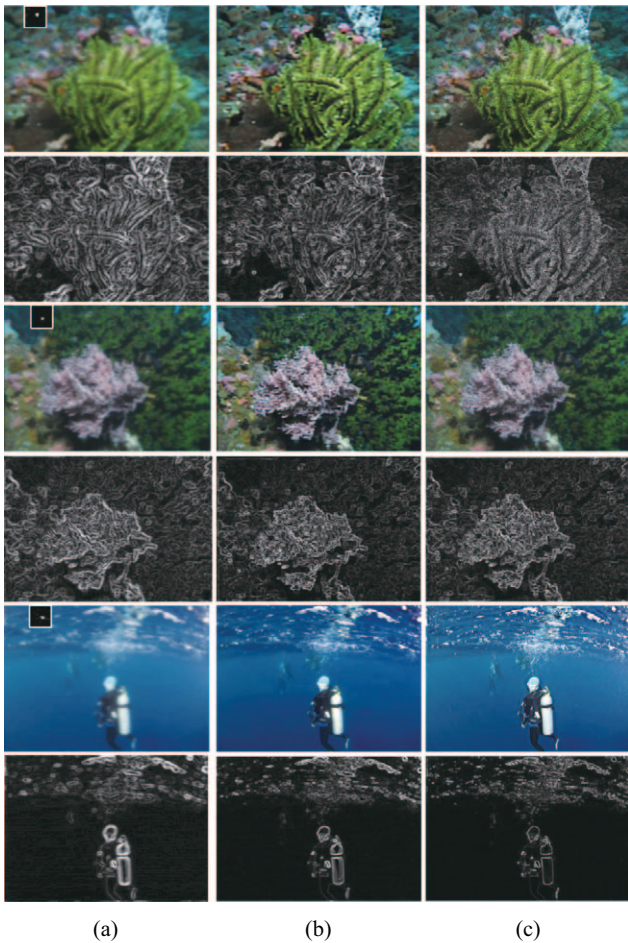
Fig. 11. (a) Observed image. (b) Enhanced image and estimated blur kernel by Pan's approach. (c) Enhanced image by proposed approach.

VI. CONCLUSION

This paper proposes a framework integrating DehazeNet and HWD together to enhance underwater images. The main contribution of this paper is that the proposed method is more robust and outperforms several state-of-the-art methods in different underwater environments. With the increasing of color distortion, DehazeNet has a more stable performance to estimate the transmission map than other haze removal algorithms. On the basis of the CDF9/7, DFBs is utilized to the high-frequency wavelet subbands. Compared with the traditional wavelets transform, HWD can obtain more the texture and contour details. A non-reference image quality assessment model is trained based on the GLCM and random forests to evaluate the performance of these algorithms comprehensively. Subjective results indicate that the algorithm can clarify images best and cause less color deviation. Objective results shows that the proposed method significantly enhances some kinds of degraded images and has the best performance in term of the GLCM features and DMOS.

ACKNOWLEDGEMENTS

REFERENCES

Ancuti, C., O., T. Haber and P. Bekaert (2012). Enhancing underwater images and videos by fusion. IEEE Conference on Computer Vision and Pattern Recognition, Providence, Rhode Island, USA, 81-88.

Cai, B., X. Xu, K. Jia, C. Qing and D. Tao (2016). Dehazenet: an end-to-end system for single image haze removal. IEEE Transactions on Image Processing 25(11), 5187-5198.

Chao, L. and M. Wang (2010). Removal of water scattering. International Conference on Computer Engineering and Technology, Chengdu, China, 35-39.

Chiang, J. Y. and Y. C. Chen (2012). Underwater image enhancement by wavelength compensation and dehazing. IEEE Transactions on Image Processing 21(4), 1756-1769.

Eslami, R. and H. Radha (2007). A new family of nonredundant transforms using hybrid wavelets and directional filter banks. IEEE Transactions on image processing 16(4), 1152-1167.

Finlayson, G. D. and E. Trezzi (2004a). Shades of gray and colour constancy. Color and Imaging Conference 5, 37-41.

Padmavathi, G., P. Subashini and M. M. Kumar (2010). Comparison of filters used for underwater image pre-processing. IJCSNS International Journal of Computer Science and Network Security 10(1), 58-65.

Galdran, A., D. Pardo, A. Picón and A. Alvarez-Gila (2015). Automatic red-channel underwater image restoration. Journal of Visual Communication & Image Representation 26, 132-145.

Goodfellow, I. J., D. Warde-Farley, M. Mirza, A. Courville and Y. Bengio (2013). Maxout Networks. Computer Science 28(3), 1319-1327.

He, K., J. Sun and X. Tang (2009). Single image haze removal using dark channel prior. IEEE Conference on Computer Vision and Pattern Recognition, Miami, Florida, USA, 1956-1963

He, K., J. Sun and X. Tang (2010). Guided image filtering. European Conference on Computer Vision, Heraklion, Crete, Greece, 1-14.

Huo, J.-Y., Y.-L. Chang and J. Wang (2006). Robust automatic white balance algorithm using gray color points in images. IEEE Transactions on Consumer Electronics 52(2), 541-546.

Iqbal, K., M. Odetayo and A. James (2010). Enhancing the low quality images using unsupervised colour correction method. IEEE International Conference on Systems Man and Cybernetics, Istanbul, Turkey, 1703-1709.

Drews-Jr, P., E. do Nascimento, F. Moraes and S. Botelho and M. Campos (2013). Transmission estimation in underwater single images. IEEE International Conference on Computer Vision Workshops, Portland, Oregon, USA, 825-830.

Lei, X. H. and K. C. Yang (2011). A gradient transfer contrast enhancement for underwater image. Journal of Naval University of Engineering 23(1), 28-31.

Liu, Z., Y. Yu, K. Zhang and H. Huang (2001). Underwater image transmission and blurred image restoration. Optical Engineering 40(6), 1125-1131.

Morillas, S., V. Gregori and A. Sapena (2006). Fuzzy bilateral filtering for color images. Image Analysis and Recognition 4141, 138-145.

Pan, J., D. Sun, H. Pfister and M. H. Yang (2016). Blind image deblurring using dark channel prior. IEEE Conference on Computer Vision and Pattern Recognition, Las Vegas, NV, USA, 1628-1636.

Sang, Q. B., C. F. Li and X. J. Wu (2013). No-reference blurred image quality assessment based on gray level co-occurrence matrix. Pattern Recognition and Artificial Intelligence 26(5), 492-497.

Schechner, Y. Y. and N. Karpel (2005). Recovery of underwater visibility and structure by polarization analysis. IEEE Journal of Oceanic Engineering 30, 570-587.

Tan, C. S., A. L. Sluzek and T. Y. Jiang (2007). Range gated imaging system for underwater robotic vehicle. OCEANS, Aberdeen, Britain, 1-6.

Tang, K., J. Yang and J. Wang (2014). Investigating haze-relevant features in a learning framework for image dehazing. IEEE Conference on Computer Vision and Pattern Recognition, Columbus, Ohio, USA, 2995-3002.

Thakur, V. and N. Tripathi (2010). On the way towards efficient enhancement of multi-channel underwater images. International Journal of Applied Engineering Research 5(5), 895-903.

Voss, K. J. and A. L. Chapin (1990). Measurement of the point spread function in the ocean. Applied Optics 29(25), 3638-3642.

Zhang, S., P. Zeng, X. Luo and H. Zheng (2012). Multi-scale retinex with color restoration and detail compensation. Journal of Xian Jiaotong University 46(4), 32-37.